Tube-width fluctuations of entangled stiff polymers

Jens Glaser* and Klaus Kroy
Institut für Theoretische Physik, Universität Leipzig, PF 100920, D-04009 Leipzig, Germany
(Received 27 November 2010; revised manuscript received 28 September 2011; published 1 November 2011)

The tubelike cages of stiff polymers in entangled solutions have been shown to exhibit characteristic spatial heterogeneities. We explain these observations by a systematic theory generalizing previous work by Morse [Phys. Rev. E **63**, 031502 (2001)]. With a local version of the binary collision approximation, the distribution of confinement strengths is calculated, and the magnitude and the distribution function of tube radius fluctuations are predicted. Our main result is a unique scaling function for the tube radius distribution, in good agreement with experimental and simulation data.

DOI: 10.1103/PhysRevE.84.051801 PACS number(s): 61.25.H−, 82.35.Pq, 87.16.Ln

I. INTRODUCTION

Entangled solutions of stiff polymers are minimal model systems to generate a fundamental understanding of the origin of the mechanical properties of the cytoskeleton. This complex polymer scaffold maintains the stability and integrity of animal cells and is composed of three types of semiflexible biopolymers, microtubules, actin, and intermediate filaments, with backbone diameters in the nanometer range but persistence lengths on the order of 10^{-1}–10^{3} μm [1–3]. Single biopolymers exhibit a rich mechanical response [4–7]. *In vitro* reconstituted solutions of such biopolymers hint at how cells can acquire a considerable macroscopic strength from a purely topological microscopic constraint and thermal fluctuations, utilizing a minimum amount of material. Though the individual polymers only have to respect a simple constraint, namely the mutual impenetrability of the polymer backbones, complex soft-solid mechanical behavior arises at densities that would correspond to a very dilute gas without polymerization and a certain flexibility allowing for thermal backbone undulations. To deform an entangled polymer, surrounding polymers need to be pushed out of the way, as familiar from knotted strings. This mechanism leads to confinement of the individual polymers in effective tubelike cages, from which they only escape very slowly by a snakelike motion called reptation [8,9]. The suppression of chain motion perpendicular to the tube backbone is responsible for the remarkable integrity of the transient network. A microscopic derivation of this confinement poses formidable theoretical challenges, and there has so far been little progress beyond the introduction of basic topological invariants characterizing polymer entanglement [10,11] and a phenomenological primitive path analysis [12].

Nevertheless, self-consistent approximations for the dynamics of rigid [13,14] and the equilibrium statistical mechanics of semiflexible [15] topologically entangled chains have been worked out, and these treatments can predict salient properties of the reptation dynamics and the postulated tube. For stiff but not rigid polymers, with a large but finite persistence length l_p, the tube confinement of the transverse fluctuations of a representative test chain is implemented by a harmonic potential of stiffness ϕ. The confinement geometry is characterized by an entanglement (or collision) length $L_e \ll l_p$ and the tube width $R \ll L_e$ [16,17], both of which are functions of ϕ. The former is a measure of the average spacing between adjacent collisions with background polymers, each of which contribute an amount k_BT to the average confinement energy of the test chain. The latter measures the magnitude of the confined thermal fluctuations (Fig. 1). Its mean value $\overline{R}$ as a function of monomer concentration has been predicted theoretically based on a binary collision approximation (BCA) and an effective medium approximation (EMA) [15]. The BCA focuses on the pairwise entanglement topology of a test chain, while the EMA aims to account for the collective network fluctuations. More recently, these mean-field type theories have been challenged by the observation of pronounced heterogeneities of the local tube width $R(s)$ along the tube contour, which have been systematically studied in experiments [18–22] and in simulations [23]. The tube heterogeneities have been statistically quantified by a broad and skewed tube width distribution $P(R)$, which has been analyzed by an empirical model [21] and by a generalization of the BCA [22].

In the following, we develop a systematic, BCA-based theory to describe the fluctuations of the tube radius in an entangled polymer solution on the scale of individual tube collisions. Thereby, the local tube radius heterogeneities $R(s)$ and their distribution $P(R)$ can be determined, and $P(R)$ is found to be a universal non-Gaussian scaling function with a stretched tail. By comparison with the segment fluid approach of Ref. [22], in which the entangled solution is effectively mapped onto an ensemble of entanglement segments, we predict the segment length L (which was previously treated as a fit parameter). The magnitude of the tube width fluctuations is compared with published experimental data. In Ref. [21], $P(R)$ was instead estimated based on an *ad hoc* distribution of the local mesh size. The result turned out to be unphysical at small values of R, however. As we show in the following, the fluctuations of the tube radius R can be comprehensively described without additional assumptions based on a generalization of the BCA.

The remainder of the paper is organized as follows. In Sec. II, we introduce the fundamental concept of the tube and the wormlike chain (WLC) model for a single confined semiflexible polymer. In Sec. III, we then summarize the basic

*Present address: CEMS, University of Minnesota, 421 Washington Avenue SE, Minneapolis, MN 55455; jglaser@umn.edu

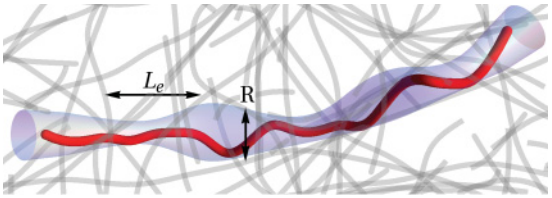

FIG. 1. (Color online) Test polymer in a background solution, confined into a tube of spatially varying radius $R(s)$. The chemical distance L_e indicates the characteristic scale of the tube heterogeneities.

assumptions underlying the BCA as an approximation to the topological problem. Subsequently, in Sec. IV, we discuss the statistical distribution of the confinement strength, which explains the fluctuations of the tube radius, that are derived in Sec. V. In Sec. VI, the magnitude of tube radius fluctuations is used as an input to the segment fluid model, which predicts a scaling function for the tube radius distribution $P(R)$. The analytical results are compared to experimental data in Sec. VII.

II. BASIC ELEMENTS OF THE TUBE MODEL

A. Time scale separation and topology

We consider a stiff test polymer in the presence of surrounding uncrossable polymers, which are imposing topological constraints on its conformation. We restrict our discussion to tightly entangled polymers that are characterized by small transverse excursions around an average path—the preferred contour. The tube concept concerns quantities in an intermediate equilibrium, i.e., on time scales $\tau_e \ll t \ll \tau_d$, where τ_e is the time for the confined degrees of freedom to equilibrate inside the tube and τ_d is the disengagement time of the polymer from its initial tube. In what follows, a strong scale separation $\tau_e \ll \tau_d$ is assumed. Then, in the idealized limit $\tau_d \to \infty$, the topological relationships of the solution will be asymptotically conserved, and the average positions of the background polymers and their mutual topological relationships can be considered as effectively frozen (or "quenched"), thus collectively giving rise to a (quasistatic) confinement potential representing the tube. We denote the thermal average with respect to a given quenched configuration by angular brackets $\langle\cdots\rangle$ and the average over different configurations and topologies of the tube by an overbar $\overline{\cdots}$. These ensemble averages correspond to temporal averages over several time intervals of length τ_e and τ_d, respectively.

B. Statistical mechanics of a single entangled stiff polymer

1. Transverse distance distribution

To describe the physical properties of the test polymer, we assume that the effect of confinement can, to leading order, be described by a harmonic confinement potential. Hence we use the weakly bending Hamiltonian

$$H_{\rm conf} = \frac{l_p}{2}\int ds\left[\frac{d^2\mathbf{r}_\perp(s)}{ds^2}\right]^2 + \frac{1}{2}\int ds\,\phi(s)\mathbf{r}_\perp^2(s) \qquad (1)$$

for the transverse fluctuations $\mathbf{r}_\perp(s)$ of the test polymer about the straight ground state of a rigid rod, with a local confinement strength $\phi(s)$ that will be determined self-consistently. We use natural energy units ($k_BT = 1$), such that the persistence length $l_p = \kappa/k_BT$ is synonymous with the bending rigidity κ. We define the arc-length dependent tube radius $R(s)$ via the variance of one component of the confined transverse fluctuations,

$$R^2(s) \equiv \tfrac{1}{2}\langle \mathbf{r}_\perp^2(s)\rangle. \qquad (2)$$

Approximating the free energy by an effective Hamiltonian $H_{\rm conf}$ that is quadratic in the fluctuations $\mathbf{r}_\perp(s)$ is equivalent to approximating the distribution of $P[\mathbf{r}_\perp(s)]$ in a given configuration by a Gaussian. Experiments [19,21,22] and simulations [23,24] indicate that the distribution of transverse distances is indeed Gaussian for small transverse displacements $\mathbf{r}_\perp(s)$ on the order of the tube radius R. It can be shown theoretically that this assumption is in accord with a self-consistent treatment of the tube [15].

2. Tube radius R and entanglement length L_e

As a first step, we consider the case of a test polymer in a homogeneous (cylindrical) tube that can be characterized by the spatial average $\overline{\phi}$ of a local confinement strength $\phi(s)$, and hence a tube radius $R(s) \equiv R_0 = \text{const}$. The variance of $\mathbf{r}_\perp(s)$ [Eq. (2)] is obtained from the tube Hamiltonian Eq. (1) via equipartition, such that

$$R^2(s) = \int \frac{dq}{2\pi}\frac{1}{l_pq^4 + \overline{\phi}} \qquad (3)$$

$$= \frac{1}{2\sqrt{2}l_p^{1/4}\overline{\phi}^{3/4}} \equiv R_0^2 \qquad (4)$$

is the square of the tube radius corresponding to a homogeneous confinement strength $\overline{\phi}$. Heterogeneities of the tube potential and of the tube radius are discussed below (in Secs. IV and V), where we show how small spatial fluctuations $\delta\phi(s) \equiv \phi(s) - \overline{\phi}$ lead to spatial variations of $R(s)$ about its average value $\overline{R}$. We assume in what follows that the peak of the corresponding distribution $P(R)$ is sufficently well defined such that the average $\overline{R}$ and the typical value R_0 can be used interchangeably.

The second characteristic quantity of the tube geometry, the entanglement length L_e, is defined by assigning a harmonic confinement energy equal to k_BT (=1 in our units) to every collision, and identifying L_e with the collision length. Writing $\overline{\phi}$ for the average confinement potential strength in Eq. (1), equipartition yields

$$L_e = \left[\int \frac{dq}{2\pi}\frac{\overline{\phi}}{l_pq^4 + \overline{\phi}}\right]^{-1} = 2\sqrt{2}\frac{l_p^{1/4}}{\overline{\phi}^{1/4}}. \qquad (5)$$

III. BCA

We recapitulate the essential arguments that are needed to derive the BCA and to understand the reasoning that follows.

The BCA was designed as an approximation to the underlying topological many-body problem, suitable for estimating the absolute value of the average tube radius $\overline{R}$ self-consistently. One considers an elementary encounter ("binary collision") between two tubes, calculates the free energy of

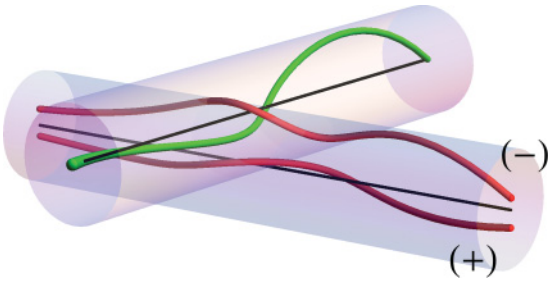

FIG. 2. (Color online) Topology of two confined polymers inside their tubes at a collision point: for fixed preferred tube contours in the transparent state, the polymers are found either in the "above" (+) or "below" (−) configuration. Adapted from Ref. [15].

confinement due to the uncrossability of the chains, and sums over possible configurations of the pair of tubes. The key approximation consists in neglecting correlations between multiple collisions.

The dynamic entanglement problem is cast into equilibrium statistical mechanics language by assuming that the tube contours are (temporarily) frozen. In such a configuration, an arbitrarily chosen point on the tube contour associated with the test chain is characterized by a Gaussian distribution of transverse distances, as outlined in the preceding section. Its standard deviation is approximated by the average tube radius $\overline{R}$. Consider now a second background chain passing within a distance $\overline{R}$ from the chosen point on the test chain. We refer to this event as a tube collision. To calculate the contribution of the pair collision to the confinement free energy, the BCA distinguishes between two states: a hypothetical state, in which the test chain is transparent with respect to collisions with the background chain and a state in which the chains are mutually uncrossable. Due to the key assumption that the collisions along the test chain are uncorrelated, the environment of the collision point is completely random in the transparent state, i.e., the distribution of transverse distances is unchanged from the Gaussian distribution with standard deviation $\overline{R}$. The average free energy of confinement follows from a topological argument. In the uncrossable state for this pair of chains, the configuration space of transverse fluctuations is divided into two disconnected subspaces corresponding to the above (+) and the below (−) configuration, as depicted in Fig. 2. The average free energy in the uncrossable state is therefore obtained by averaging the confinement potential in each of these subspaces over the probability for a specific topology and collision geometry. The resulting effective potential is equated with that of the transparent state to obtain a self-consistent estimate of the tube radius $\overline{R}$.

For the original mathematical implementation of the above ideas, we refer the reader to Ref. [15]. We note that a slightly corrected estimate for the prefactor in the scaling result for the average tube radius $\overline{R}$ with concentration was calculated in Ref. [22] (supplement).

IV. DISTRIBUTION $P[\phi]$ OF TUBE STRENGTHS

The original BCA is exclusively concerned with average values $\overline{R}$, $\overline{\phi}$. The scaling of these values with concentration ρ has been tested experimentally [20,21,25], but the prefactor is sensitive to the precise control of the experimental conditions and is usually treated as a fit factor. For a more detailed comparison of theory, experiment, and simulations, knowledge not only of the average value but of the richer and more robust tube radius distribution $P(R)$ is desirable (cf. Sec. V).

As a first step toward calculating $P(R)$, we derive the distribution $P[\phi]$ of the local confinement strength $\phi(s)$ of a test polymer. Morse [15] gave an explicit expression for the confinement free energy of a test chain colliding with a medium chain. We will explicitly adopt the mathematical approximation of straight tube contours that was implicitly made in the previous work, and it is shown that inconsistencies resulting from this approximation are avoided by verifying that the calculated quantities do not depend on the overall chain length. Let the distance of shortest approach between two preferred contours with orientations $\mathbf{u}$, $\mathbf{u}'$ and centers of mass $\mathbf{r}$, $\mathbf{r}'$ be $x = (\mathbf{r} - \mathbf{r}') \cdot \mathbf{e}_x$, where $\mathbf{e}_x = \mathbf{u} \times \mathbf{u}'/|\mathbf{u} \times \mathbf{u}'|$ is the direction perpendicular to both preferred contours; then the free energy of the test polymer whose preferred contour has been uniformly displaced by a vector $\mathbf{h} = h\mathbf{e}_h$ is

$$F_{\pm}(\mathbf{h}) = -\ln \Phi\left(\pm \frac{x - h\,\cos\psi}{\overline{R}}\right). \tag{6}$$

Here the sign $\pm$ refers to the specific topology (cf. Fig. 2) and $\cos\psi = \mathbf{e}_h \cdot \mathbf{e}_x$. The function $\Phi(y)$ is given by the restricted partition sum of the Gaussian fluctuations of the test polymer in the presence of an uncrossable test chain [15],

$$\Phi(y) = \frac{1}{2}\mathrm{erfc}\left(-\frac{y}{2}\right). \tag{7}$$

It can be interpreted as the probability $p_{\pm}(x) = \Phi(\pm x/\overline{R})$ of finding a specific topology.

From Eq. (6), we obtain the confinement strength ϕ in a given configuration of preferred contours and topology as the second derivative of the free energy,

$$\phi_{\pm}(x) = \frac{d^2}{dh^2} F_{\pm}(\mathbf{h})\bigg|_{h=0} = -\frac{\cos^2\psi}{\overline{R}^2}\frac{d^2}{dy^2}\ln\Phi(y)\bigg|_{\pm x/\overline{R}}. \tag{8}$$

To derive the distribution of confinement strengths $\phi(s)$, we now turn back to the central BCA approximation that the collisions between the test polymer and the background polymers are independent localized events. Due to the requirement $\overline{R} \ll L_e$, we may, without loss of generality, even treat them as pointlike and express the confinement potential $\phi(s)$ per unit length at a point s on the test polymer as

$$\phi(s) = \sum_{i=1}^{N} \chi(\mathbf{r}_i, \mathbf{u}_i, \mathbf{u})\delta(s - z_i)\phi_{\pm}(x_i). \tag{9}$$

Here $\chi(\mathbf{r}_i, \mathbf{u}_i, \mathbf{u})$ is a characteristic function of overlap between the colliding tubes, which takes on the value one whenever a tube collision occurs, and zero otherwise (for a graphical definition, see Fig. 3). We introduce it here merely as a convenient tool to facilitate the formal manipulation of the following expressions. The coordinate z_i in the argument of the δ function is the point of shortest approach (the collision point) between the two tubes on the test polymer.

The distribution $P[\phi]$ of confinement strengths that follows from Eq. (9) is of the Holtsmark type [26,27] and describes

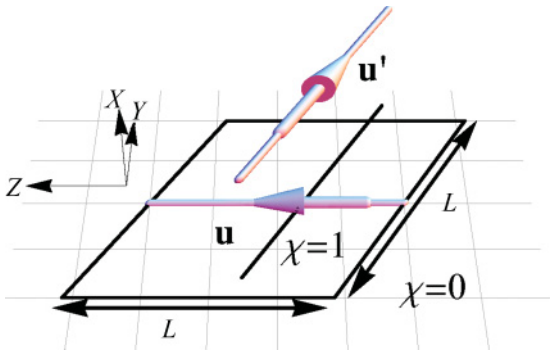

FIG. 3. (Color online) Overlap area (parallelogram) of two tubes of length L, represented by their preferred contours with orientations $\mathbf{u}$, $\mathbf{u}'$ enclosing an arbitrary angle, and characteristic function χ.

the total confinement potential of the test chain as a sum of contributions resulting from uncorrelated collisions with medium chains. Explicitly, its moment-generating functional is given by (cf. Appendix A)

$$P[w(s)] = \exp\left[\frac{n}{2\pi}\sum_{\pm}\int \mathbf{dr}'\int' d\mathbf{u}'\,\chi\, e^{i\,w(z')\phi_{\pm}(x')}p_{\pm}(x')\right]. \tag{10}$$

From this, we obtain the average of $\phi(s)$ by functional differentiation of the logarithm of Eq. (10) with respect to the field $w(s)$ (cf. Appendix A),

$$\overline{\phi} = \frac{nL\pi}{8\overline{R}}\int dy\,\frac{\Phi'^2(y)}{\Phi(y)}. \tag{11}$$

The integral in Eq. (11) is numerically evaluated and gives $\overline{\phi} = \alpha nL/\overline{R}$, with $\alpha = 0.502$, in agreement with earlier results [15] (applying the slight numerical correction discussed in Ref. [22], supplement).

We proceed analogously to obtain the second cumulant (cf. Appendix A), the correlation function

$$\overline{\phi(s)\phi(s')} = \beta\frac{nL}{\overline{R}^3}\delta(s-s'), \tag{12}$$

where $\beta = 0.0941$. The uncorrelated character of the collisions is apparent from the δ function on the right-hand side of Eq. (12). Both should be understood in the coarse-grained sense, assuming $\overline{\phi(s)\phi(s')} = 0$ when $s - s' \gg \overline{R}$.

V. GAUSSIAN APPROXIMATION TO THE TUBE RADIUS DISTRIBUTION $P(R)$

We can now turn the distribution $P[\phi]$, which we characterized by its first two cumulants, into a Gaussian approximation to the tube radius distribution $P(R)$, by calculating the linear response of the local tube radius $R(s)$ to spatial changes (heterogeneities) in $\phi(s)$. We begin with the observation that the correlation function of the (projected) transverse fluctuations, $C(s,s') = \langle \mathbf{r}_\perp(s)\cdot\mathbf{r}_\perp(s')\rangle/2$, obeys the following differential equation (cf. Appendix B):

$$-l_p\partial_s^4 C(s,s') - \phi(s')C(s,s') = \delta(s-s'). \tag{13}$$

The tube radius is given by $R(s) = [C(s,s)]^{1/2}$ and the linear response expression for this quantity is calculated in Appendix B as

$$R(s) = \overline{R} - \frac{1}{2\overline{R}}\int ds'\,G^2(s-s')\delta\phi(s'). \tag{14}$$

The variance of the tube radius $R(s)$ at a randomly chosen point s on the test polymer is now calculated from Eq. (14) as

$$\overline{\delta R^2} \equiv \overline{[R(s)-\overline{R}]^2} = \frac{1}{4\overline{R}^2}\int ds'ds''\,G^2(s-s')G^2(s-s'')\overline{\phi(s')\phi(s'')}. \tag{15}$$

Within the BCA, with its trivial spatial correlations of the confinement potential $\phi(s)$, Eq. (12), this reduces to

$$\overline{\delta R^2} = \beta\frac{nL}{4\overline{R}^5}\int ds'G^4(s-s'). \tag{16}$$

The integral Eq. (16) is numerically evaluated using an explicit expression for $G(s)$ [Eq. (B5)],

$$\int ds\,G^4(s) = \gamma\overline{R}^8 L_e, \tag{17}$$

where $\gamma = 0.5125$, which yields the final result for the variance of $P(R)$,

$$\overline{\delta R^2} = \tfrac{1}{4}\beta\gamma nL\overline{R}^3 L_e. \tag{18}$$

Using the self-consistent solutions for $\overline{R} = (4\alpha)^{-3/5}(nL)^{-3/5}l_p^{-1/5}$ and $L_e = (\alpha/8)^{-2/5}(nL)^{-2/5}l_p^{1/5}$ [15], mean and variance of the Gaussian approximation to the tube radius distribution $P(R)$ are completely determined in terms of the contour length concentration nL and the persistence length l_p. In particular, the coefficient of variation $c_v = [\overline{\delta R^2}]^{1/2}/\overline{R}$ turns out to be a concentration-independent constant,

$$c_v = \frac{1}{2}\sqrt{\frac{\beta\gamma}{\alpha}} = 0.155. \tag{19}$$

VI. SEGMENT FLUID APPROXIMATION

In Ref. [22], a broad distribution $P(R)$ of the tube radius was found. The derivation of an analytical result for this distribution was also based on a Holtsmark-type distribution for the confinement strength ϕ resulting from uncorrelated collisions, but the latter were averaged over the characteristic length L of entanglement segments (which is why the approach was called a "segment-fluid" approximation). It was argued that this length is on the order of L_e. We now show that this choice is indeed justified and predict the precise value of the segment length.

The tube radius distribution $P(R)$ was given as an analytical approximation in Ref. [22],

$$P(R) = \frac{8}{3R\Gamma(k)}\exp(-y)y^k, \quad y \equiv 0.01325\frac{L\overline{R}^2}{\ell_p^{1/3}R^{8/3}}, \tag{20}$$

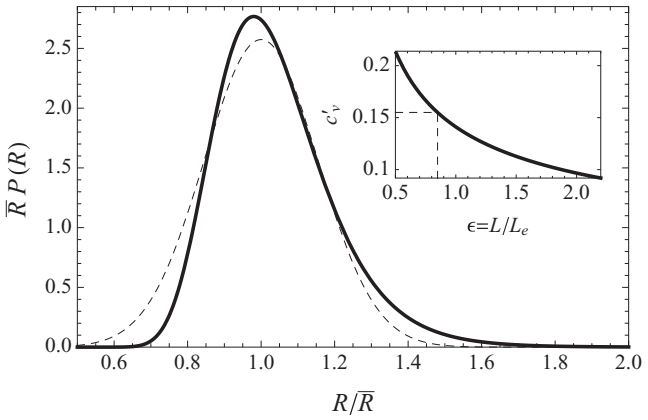

FIG. 4. Reduced distribution $\overline{R}P(R)$ of the tube radius R. The solid line is the segment-fluid prediction; the dashed line is a Gaussian approximation with coefficient of variation c_v given by Eq. (19). Inset: Coefficient of variation c_v' of the segment fluid approximation vs reduced segment length $\epsilon = L/L_e$, and the predicted value.

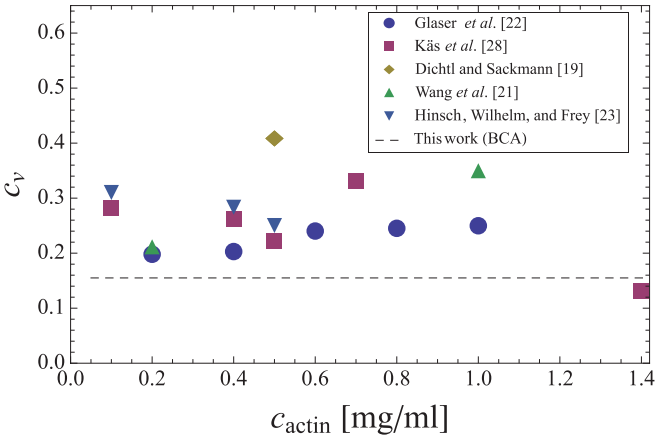

FIG. 5. (Color online) Comparison of tube radius fluctuations in different experiments and simulations of semidilute solutions of F-actin. Shown is the coefficient of variation $c_v = \sqrt{\overline{\delta R^2}}/\overline{R}$ for the fluctuations of R. Symbols correspond to data taken from the literature. Circles: experimental data taken from Ref. [22] (Fig. 3, inset); squares: experimental data from Ref. [28]; diamonds: experimental data from Ref. [19] for the fluctuations of the response coefficient $\alpha_\perp$, converted to fluctuations of the tube radius R; upright triangles: experimental data from [21] (Fig. 2); downward facing triangles: simulation data from Ref. [23] (Fig. 9). The solid dashed line is the prediction of Eq. (19).

where $k = 4.013n'L^2\overline{R}$, n' is the number density of entanglement segments, and $\Gamma(x)$ is the Γ function. It was noted [22] that $P(R)$ can be written as a scaling function $P(R) = (1/\overline{R})f(R/\overline{R}, n'L^2\overline{R})$. This implies that the coefficient of variation is given by a constant, $c_v' = g(n'L^2\overline{R})$. If we make the ansatz $L = \epsilon L_e$, with an undetermined dimensionless constant ϵ and use the self-consistent values for $\overline{R}$ and L_e given above, we get $c_v' = g(\epsilon/\alpha)$. The function $g(x)$ is easily evaluated numerically and is shown in Fig. 4 (inset). To fix ϵ and thus the length L of entanglement segments, we require $c_v' = c_v$ and obtain numerically $\epsilon = 0.85$.

Evaluating the tube radius distribution $P(R)$ [Eq. (20)] at this value of the reduced segment length L/L_e, we obtain $k = y(R/\overline{R})^{8/3} = 6.79$ and hence all parameters occurring in $P(R)$ are now fully specified, giving

$$P(R) = N \exp\left[-6.79\left(\frac{\overline{R}}{R}\right)^{8/3}\right](\overline{R}/R)^{8/3}, \qquad (21)$$

with a normalization constant $N = 2.434 \times 10^3$. The corresponding unique reduced distribution $\overline{R}P(R)$ is shown in Fig. 4 and compared to the Gaussian distribution with the same c_v. Beyond what was achieved in Ref. [22], the functional form of $P(R)$ is now fully determined. As can be seen in Fig. 4, the distribution $P(R)$ is positively skewed and has a broad tail at large values of R.

VII. COMPARISON TO EXPERIMENT

The functional form of $P(R)$ was compared to experimental data in Ref. [22], and very good qualitative agreement was found, using the value of the segment length L as a fit parameter. Remarkably, also our above prediction of a constant value for the coefficient of variation c_v, which can be checked against a whole set of independent measurements, is nicely confirmed by the data (Fig. 5).

The figure summarizes literature data for c_v against monomer concentration c from various experiments and simulations of semidilute actin solutions. The dashed line is our prediction from Eq. (19). Two results are evident from this plot. First, the data scatter within a band of $c_v = 0.2$–0.4. Second, the theoretical prediction lies below most of the data points and thus provides a lower bound for the observed tube radius fluctuations. This suggests that a constant value for the coefficient of variation is indeed consistent with the reported data, but that the heterogeneities are actually about twice as strong as predicted.

This is not entirely unexpected, since the BCA, on which our theoretical derivation relies, is not meant to describe the absolute value of the tube radius quantitatively. In fact, the BCA alone is well known to underestimate the tube fluctuations, since it does not take into account the collective fluctuations of the surrounding medium into which the tube is embedded [15]. Corresponding quantitative discrepancies with experiments have been reported before [25].

VIII. CONCLUSION

We have calculated the fluctuations of the tube radius in entangled solutions of semiflexible polymers, based on the binary collision approximation (BCA). We predict that the shape of the tube radius distribution is given by a universal (concentration-independent) scaling function, for which we gave an analytical approximation in Eq. (21). Our results provide a quantitative characterization of the local packing structure of entangled biopolymer solutions in terms of distribution functions, which are at the same time a more sensitive and more robust means for comparing data and theory than average values alone. We hope that the methods of analysis established here may find application in future experimental studies, e.g., in microrheology [29,30], or in the

interpretation of simulation data [23,31]. Further theoretical questions, such as the characterization of the distribution of tube contours [20,32], are currently under study.

ACKNOWLEDGMENTS

We are indebted to David Morse for his most valuable comments on the manuscript. We also gratefully acknowledge inspiring discussions with Lars Wolff, Dipanjan Chakraborty, Sebastian Sturm, and Andrew Gustafson. We thank Inka Lauter for providing experimental data on the tube width fluctuations of actin solutions that motivated the discussion of the tube radius distribution. This work was supported by the Deutsche Forschungsgemeinschaft (DFG) through FOR 877 and the Leipzig School of Natural Sciences—Building with Molecules and Nano-objects.

APPENDIX A: CALCULATION OF THE DISTRIBUTION OF CONFINEMENT STRENGTHS $P[\phi]$

The distribution of the local confinement strength is formally obtained as the average $P[\varphi(s)] = \overline{\delta[\phi(s) - \varphi(s)]}$ over all possible configurations of tube contours and topologies. The corresponding characteristic functional, $P[w(s)]$, follows from a functional Fourier transform and Eq. (9) as

$$P[w(s)] = \overline{\exp\left(i \sum_{i=1}^{N} \chi(\mathbf{r}_i, \mathbf{u}_i, \mathbf{u}) w(z_i) \phi_{\pm}(x_i)\right)}. \quad \text{(A1)}$$

Here tangents to the test and the background chains' tube backbones are denoted by $\mathbf{u}$ and $\mathbf{u}_i$, and the vector $\mathbf{r}_i$ connects the tubes' center of mass of the test chain with that of the background chain i. Its coordinates x_i, y_i, and z_i are defined along the directions $\mathbf{e}_{x,i} = (\mathbf{u} \times \mathbf{u}_i)/|\mathbf{u} \times \mathbf{u}_i|$, $\mathbf{e}_{y,i} = \mathbf{u} \times \mathbf{e}_{x,i}$, and $\mathbf{e}_{z,i} = \mathbf{u}$. The quenched average $\overline{\cdots}$ is implemented as the simultaneous average over the probability $p_{\pm}(x_i) = \Phi(\pm x_i/\overline{R})$ of finding a specific topology "+" or "−" [defined after Eq. (7)] and over the uniformly distributed centers of mass and orientations of the tubes. Since the chains' preferred contours are assumed to be uncorrelated, the average over the N preferred contours and the topology of the background chains relative to the test chain factorizes as

$$P[w(s)] = \left[\sum_{\pm} \int \frac{d\mathbf{r}'}{V} \int' \frac{d\mathbf{u}'}{2\pi} e^{i\chi(\mathbf{r}', \mathbf{u}', \mathbf{u}) w(z') \phi_{\pm}(x')} p_{\pm}(x')\right]^N. \quad \text{(A2)}$$

Here the integral over orientations extends over the half-sphere (indicated by a prime). Exploiting the formal definition of χ as a characteristic function of overlap, which amounts to setting the factor in the brackets for nonoverlapping chains to unity [since the probability $p_{\pm}(x')$ is normalized], we get

$$P[w(s)] = \left\{1 + \sum_{\pm} \int \frac{d\mathbf{r}'}{V} \int' \frac{d\mathbf{u}'}{2\pi} \left[e^{i w(z') \phi_{\pm}(x')} p_{\pm}(x') - 1\right] \chi\right\}^N. \quad \text{(A3)}$$

Using $n = N/V$ for the polymer number concentration and performing the limit $N \to \infty$, Eq. (10) in the main text is obtained.

The first cumulant is obtained by functional differentiation of the characteristic functional Eq. (10) with respect to the field $w(s)$,

$$\overline{\phi(s)} = -i \frac{\delta}{\delta w(s)} \ln P[w(s)]\Big|_{w(s)=0} \quad \text{(A4)}$$

$$= \frac{nL}{2\pi} \sum_{\pm} \int' d\mathbf{u}' \int d\mathbf{r}' \, \delta(z' - s) \chi p_{\pm}(x') \phi_{\pm}(x'). \quad \text{(A5)}$$

Using the fact that the integral of $\chi \delta(z' - s)$ over dy' and dz' is the height $L \sin\theta$ of the overlap area (Fig. 3), carrying out the second derivative of $-\ln \Phi$ and the angular integrals, and using $\sum_{\pm} \Phi(\pm y) = 1$, one arrives at Eq. (11) in the main text. Analogously, we obtain the second cumulant, the correlation function

$$\overline{\phi(s)\phi(s')} \quad \text{(A6)}$$

$$= -\frac{\delta^2}{\delta w(s) \delta w(s')} \ln P[w(s)]\Big|_{w(s)=0} \quad \text{(A7)}$$

$$= \frac{nL}{2\pi} \sum_{\pm} \int' d\mathbf{u}' \int d\mathbf{r}' \, \delta(z' - s) \delta(z' - s') \chi p_{\pm}(x') \phi_{\pm}^2(x'). \quad \text{(A8)}$$

Applying a similar reasoning as above to simplify the equation and numerically evaluating the remaining x integral, we obtain Eq. (12) in the main text.

APPENDIX B: HETEROGENEOUS TUBE RADIUS $R(s)$

The fluctuation-response relation Eq. (13) for the correlation function $C(s,s')$ is derived from the free energy $-\ln Z[\mathbf{f}_{\perp}(s)]$ of a confined WLC in the presence of an external transverse force $\mathbf{f}_{\perp}(s)$. The corresponding Hamiltonian is $H = H_{\text{conf}} + \int ds \, \mathbf{f}_{\perp}(s) \mathbf{r}_{\perp}(s)$. Since

$$\langle \mathbf{r}_{\perp}(s) \rangle = \frac{\delta \ln Z}{\delta \mathbf{f}_{\perp}(s)}, \quad \text{(B1)}$$

$$\langle \mathbf{r}_{\perp}(s) \mathbf{r}_{\perp}(s') \rangle = \frac{\delta \ln Z}{\delta \mathbf{f}_{\perp}(s) \delta \mathbf{f}_{\perp}(s')}\Big|_{\mathbf{f}_{\perp}(s)=0} \quad \text{(B2)}$$

$$= \frac{\delta \langle \mathbf{r}_{\perp}(s) \rangle}{\delta \mathbf{f}_{\perp}(s')}\Big|_{\mathbf{f}_{\perp}(s)=0}, \quad \text{(B3)}$$

it follows that $\mathbf{C}(s,s') \equiv \langle \mathbf{r}_{\perp}(s) \mathbf{r}_{\perp}(s') \rangle$ is the functional inverse of $\mathbf{C}(s,s')^{-1} = \delta \mathbf{f}_{\perp}(s)/\delta \langle \mathbf{r}_{\perp}(s') \rangle$. Since the force $\mathbf{f}_{\perp}(s) = -\langle \delta H_{\text{conf}}/\delta \mathbf{r}_{\perp}(s) \rangle$ producing an average displacement $\langle \mathbf{r}_{\perp}(s) \rangle$ is given by $-l_p \partial_s^4 \langle \mathbf{r}_{\perp}(s) \rangle - \phi(s) \langle \mathbf{r}_{\perp}(s) \rangle$, Eq. (13) follows by partial integration.

A solution of Eq. (13) would exactly describe the tube heterogeneities that follow from a heterogeneous confinement potential $\phi(s)$. However, no such solution is available for arbitrary $\phi(s)$. Therefore, we write $\phi(s) = \overline{\phi} + \delta\phi(s)$ with small fluctuations $\delta\phi(s)$ about the average confinement strength $\overline{\phi}$. A simple first-order perturbation scheme for $C(s,s') = C^{(0)}(s,s') + \delta C(s,s')$ is set up by requiring $C^{(0)}$ to be the response function in the homogeneous case,

where $\delta\phi(s) = 0$,

$$C^{(0)}(s-s') = G(s-s') = \int \frac{dq}{2\pi} \frac{e^{iq(s-s')}}{l_p q^4 + \overline{\phi}}. \quad \text{(B4)}$$

The explicit expression for the Fourier transform in Eq. (B4) can be obtained analytically and written [using Eqs. (4) and (5)] as

$$G(s-s') = R_0^2 e^{-2|s|/L_e} \left[\cos\left(2\frac{s}{L_e}\right) + \sin\left(2\frac{|s|}{L_e}\right)\right]. \quad \text{(B5)}$$

The leading-order response $\delta C(s,s')$ to the perturbation $\delta\phi(s,s')$ is obtained from Eq. (13) if small terms $O(\delta C \delta\phi)$ are neglected,

$$\delta C(s,s') = -\int ds'' G(s-s'')\delta\phi(s'')G(s'-s''). \quad \text{(B6)}$$

Equation (14) in the main text is obtained by writing $R(s) = \overline{R} + \delta R(s)$ with $\delta R(s) = \delta(R^2)/2\overline{R} = \delta C(s,s)/2R_0$.

[1] F. Gittes, B. Mickey, J. Nettleton, and J. Howard, J. Cell Biol. **120**, 923 (1993).
[2] H. Isambert, P. Venier, A. Maggs, A. Fattoum, R. Kassab, D. Pantaloni, and M. Carlier, J. Biol. Chem. **270**, 11437 (1995).
[3] M. Schopferer, H. Bär, B. Hochstein, S. Sharma, N. Mücke, H. Herrmann, and N. Willenbacher, J. Mol. Biol. **388**, 133 (2009).
[4] A. Ghosh, J. Samuel, and S. Sinha, Phys. Rev. E **76**, 061801 (2007).
[5] M. Emanuel, H. Mohrbach, M. Sayar, H. Schiessel, and I. M. Kulić, Phys. Rev. E **76**, 61907 (2007).
[6] O. Hallatschek, E. Frey, and K. Kroy, Phys. Rev. E **75**, 031906 (2007).
[7] B. Obermayer and E. Frey, Phys. Rev. E **80**, 040801(R) (2009).
[8] S. F. Edwards, Proc. Phys. Soc. London **92**, 9 (1967).
[9] P. G. de Gennes, J. Chem. Phys. **55**, 572 (1971).
[10] S. F. Edwards, Proc. Phys. Soc. **91**, 513 (1967).
[11] K. K. Müller-Nedebock and S. F. Edwards, J. Phys. A: Math. Gen. **32**, 3283 (1999).
[12] R. Everaers, S. K. Sukumaran, G. S. Grest, C. Svaneborg, A. Sivasubramanian, and K. Kremer, Science **303**, 823 (2004).
[13] D. M. Sussman and K. S. Schweizer, Phys. Rev. E **83**, 061501 (2011).
[14] D. M. Sussman and K. S. Schweizer, Phys. Rev. Lett. **107**, 078102 (2011).
[15] D. C. Morse, Phys. Rev. E **63**, 031502 (2001).
[16] T. Odijk, Macromolecules **1344**, 1340 (1983).
[17] A. N. Semenov, J. Chem. Soc., Faraday Trans. **82**, 317 (1986).
[18] J. Käs, H. Strey, and E. Sackmann, Nature (London) **368**, 226 (1994).
[19] M. Dichtl and E. Sackmann, New J. Phys. **1**, 18 (1999).
[20] M. Romanowska, H. Hinsch, N. Kirchgeßner, M. Giesen, M. Degawa, B. Hoffmann, E. Frey, and R. Merkel, Europhys. Lett. **86**, 26003 (2009).
[21] B. Wang, J. Guan, S. M. Anthony, S. C. Bae, K. S. Schweizer, and S. Granick, Phys. Rev. Lett. **104**, 118301 (2010).
[22] J. Glaser, D. Chakraborty, K. Kroy, I. Lauter, M. Degawa, N. Kirchgeßner, B. Hoffmann, R. Merkel, and M. Giesen, Phys. Rev. Lett. **105**, 037801 (2010).
[23] H. Hinsch, J. Wilhelm, and E. Frey, Eur. Phys. J. E: Soft Matter **24**, 35 (2007).
[24] Q. Zhou and R. Larson, Macromolecules **39**, 6737 (2006).
[25] M. Tassieri, R. M. L. Evans, L. Barbu-Tudoran, G. N. Nasir Khaname, J. Trinick, and T. A. Waigh, Phys. Rev. Lett. **101**, 198301 (2008).
[26] J. Holtsmark, Ann. Phys. **363**, 577 (1919).
[27] S. H. Simon, V. Dobrosavljevic, and R. M. Stratt, J. Chem. Phys. **02912**, 2640 (1990).
[28] J. Käs, H. Strey, J. X. Tang, D. Finger, R. Ezzell, E. Sackmann, and P. A. Janmey, Biophys. J. **70**, 609 (1996).
[29] T. A. Waigh, Rep. Prog. Phys. **68**, 685 (2005).
[30] D. Wirtz, Annu. Rev. Biophys. **38**, 301 (2009).
[31] S. Ramanathan and D. C. Morse, Phys. Rev. E **76**, 010501(R) (2007).
[32] H. Hinsch and E. Frey, Chem. Phys. Chem. **10**, 2891 (2009).